Ecological communities from random generalized Lotka-Volterra dynamics with nonlinear feedback

Laura Sidhom*
Theoretical Physics, Department of Physics and Astronomy, School of Natural Sciences, The University of Manchester, Manchester M13 9PL, United Kingdom

Tobias Galla†
Theoretical Physics, Department of Physics and Astronomy, School of Natural Sciences, The University of Manchester, Manchester M13 9PL, United Kingdom
and Instituto de Física Interdisciplinar y Sistemas Complejos, IFISC (CSIC-UIB), Campus Universitat Illes Balears, E-07122 Palma de Mallorca, Spain

(Received 18 September 2019; revised manuscript received 27 January 2020; accepted 28 January 2020; published 2 March 2020)

We investigate the outcome of generalized Lotka-Volterra dynamics of ecological communities with random interaction coefficients and nonlinear feedback. We show in simulations that the saturation of nonlinear feedback stabilizes the dynamics. This is confirmed in an analytical generating-functional approach to generalized Lotka-Volterra equations with piecewise linear saturating response. For such systems we are able to derive self-consistent relations governing the stable fixed-point phase and to carry out a linear stability analysis to predict the onset of unstable behavior. We investigate in detail the combined effects of the mean, variance, and covariance of the random interaction coefficients, and the saturation value of the nonlinear response. We find that stability and diversity increases with the introduction of nonlinear feedback, where decreasing the saturation value has a similar effect to decreasing the covariance. We also find cooperation to no longer have a detrimental effect on stability with nonlinear feedback, and the order parameters mean abundance and diversity to be less dependent on the symmetry of interactions with stronger saturation.

DOI: 10.1103/PhysRevE.101.032101

I. INTRODUCTION

The discussion whether large ecosystems can maintain stability and diversity or not has a long tradition [1–3]. While models with random interaction parameters were introduced more than 45 years ago by May [4,5], they continue to play an important role in this diversity-stability debate. Models with random coupling coefficients are used not only for the modeling of large-scale ecosystems, but also to describe interactions in the human microbiome. For example, recent studies have examined how different types of interactions between microbe species, and between the human host and the microbes can affect stability [6,7].

Several approaches have been taken to study the stability of ecological communities with random interaction matrices. One is concerned with assemblies with a fixed given size, S, and assumes that their interactions are set by a random matrix. More precisely, these models focus on the study of the eigenvalues of a putative $S \times S$ Jacobian matrix, which is assumed to be random. This line of approach has been taken, for example, in Refs. [4,5] and in Refs. [8–13]. Knowledge and ideas from statistical physics contribute to these studies, exploiting technology developed for random-matrix problems, for example, in nuclear physics, the theory of disordered systems or condensed matter physics [14].

A second approach focuses on *dynamical* models of species interaction. These are often based on coupled differential equations, governing the abundances of species and their interactions. Typical examples are generalized Lotka-Volterra equations, or closely related, replicator dynamics of evolutionary game theory. These involve a definition of reproductive growth rate, which in turn requires a notion of species-to-species interaction. One assumes, for example, pairwise interaction with fixed random coefficients. Several dynamical assembly approaches can then be taken, such as the step-wise assembly process. This has been studied in simulations [15] and also analytically [16]. We use a separate approach, initiated originally in Ref. [17]. We start from a pool of species, who interact through a generalized Lotka-Volterra dynamics. In the course of these dynamics some species may become extinct, and we are interested in the community of remaining species. Given the fixed interaction coefficients, such models are dynamical problems with quenched disorder in the language of the theory of disordered systems (for a general reference see Ref. [18]).

Tools from equilibrium and nonequilibrium statistical physics can then be used to make analytical progress, usually relying on the assumption that the number of species in the system is large; formally the thermodynamic limit of an infinite number of species is taken. Different types of

*laura.sidhom@postgrad.manchester.ac.uk
†tobias.galla@manchester.ac.uk

behavior can then be found, both in simulations and from analytical approaches. For example, dynamical systems of this type can approach stable fixed points, and in suitable parameter regimes these fixed points are found to be unique, i.e., independent of the initial conditions. For other parameters multiple fixed points or equilibria can be found. Their number and statistics can be characterized, for example, using Gardner-type calculations [19,20].

Static approaches to ecosystems are based on the celebrated replica method [21–23]; this assumes the existence of a Liapunov function and typically requires a symmetric interaction matrix. A separate approach uses the cavity method or the Thouless-Anderson-Palmer (TAP) equations, again originally developed in the context of spin glasses (see, e.g., Ref. [18]). The focus here is not on the actual dynamics of the ecosystem, but on the statistics of fixed points, and on their stability [24–26]. The advantage relative to the replica approach is that symmetry of the interaction matrix is not required.

Finally, dynamic generating functionals (path integrals) have been used to study large ecosystems with disordered couplings. These techniques were originally developed for spin systems [27–29] (for more recent reviews see Refs. [30–32]) and then first applied to replicator dynamics by Opper and Diederich [17] and by Berg and Weigt [20]. This was then further developed in Refs. [33–37]. The path-integral approach is dynamic, in principle, and results in an effective process for a representative species. This dynamic mean-field theory describes the time evolution of a typical degree of freedom after the average over the quenched disorder has been carried out. In most cases this effective process involves a non-Markovian retarded interaction kernel and colored noise. This makes analytical solution difficult, in particular in transient regimes when dynamic order parameters are time dependent.

The effective dynamics resulting from the generating-functional analysis can be studied numerically using the method by Eissfeller and Opper [38] to simulate sample paths of the effective dynamics; see also Ref. [39] for further recent developments of methods to evaluate dynamical mean field theory. Analytical solutions are feasible when model parameters are such that the system converges to a unique stable fixed point, independent of the initial condition. It is then possible to derive self-consistent relations for the statistics of these fixed points and macroscopic order parameters. In the context of ecological communities these order parameters represent, among others, the fraction of species which survive the in the long run, the diversity of these species (e.g., the species abundance distribution), and the mean abundance at the fixed point.

The theory also self-consistently predicts its own instability, i.e., from the fixed-point solutions one can identify combinations of parameters at which dynamical instabilities set in. A number of different concepts of stability are used in the ecology literature [40,41]. In this paper we are mainly interested in identifying the parameter regime in which the dynamics is globally stable, i.e., it reaches one unique fixed point, irrespective of the initial condition. As we will briefly discuss later the type of instability we identify using the generating-functional approach can be related to so-called "structural stability" in ecology [16,42].

Outside the globally stable regime one finds phases in which the dynamics converge to stable fixed points, but where different fixed points are reached for different starting points of the dynamics. We also find phases with persistent dynamics, such as limit cycles, heteroclinic cycles, and chaos. For generalized Lotka-Volterra equations with random coupling matrices, finally, phases with unbounded growth can be identified [24–26,43]. Similar behavior has also been seen in the context of replicator equations [33]; we note that unbounded growth is not possible for replicator equations.

Most existing generating-functional studies of replicator or generalized Lotka-Volterra models focus on cases in which the resulting effective process takes a simple form, resulting in linear fixed-point relations. These are typically models in which the (relative) growth of the abundance of one species depends linearly on the abundances of the other species. Examples can be found in Refs. [17,33,43]. One notable exception are so-called Sato-Crutchfield dynamics in the context of game learning [44,45]. This describes situations in which players update their mixed strategies in response to moves by their opponents and payoffs received. For the learning models in Refs. [44,45] mixed strategies evolve in a way similar to species abundances in a population, but the fixed-point relations contain logarithmic terms.

In this paper we focus on an example of nonlinear feedback. This is inspired by the idea that the influence on growth from interactions with other species may not have an unlimited effect but instead saturate. This type of nonlinear feedback is often modeled using Hill functions [46], similar to Holling type-II functional response [47] in ecology. The aim of our work is to investigate how this type of nonlinear feedback affects the outcome of evolution of ecosystems with random interactions. Specifically we focus on the effects of the nonlinear feedback on the phase of global stability. We show that the saturation of feedback increases the region with a unique stable fixed point. This stabilizes communities, and leads to more diversity than in the absence of saturation.

The remainder of this paper is organized as follows. In Sec. II we define the general class of models we will be looking at, and we introduce the main control parameters. We then present results from numerical simulations of random generalized Lotka-Volterra communities with nonlinear feedback in Sec. III; in particular, we report the different types of behaviours seen and how the main model parameters influence this behavior. In Sec. IV we then develop the generating functional for the model with general feedback function, report the resulting effective species process, and the self-consistent equations characterizing the regime of unique stable fixed points. To make further analytical progress we then focus on the case of piecewise linear saturating functional feedback, and carry out a linear stability analysis. The predictions from the theory are tested in Sec. V, where we report detailed phase diagrams obtained from the path-integral analysis and from simulations. We then compare our results from the piecewise linear feedback function to results from simulations of the model with nonlinear feedback in Sec. VI. In Sec. VII we discuss the role of the different ecological parameters and, in particular, how saturation in the nonlinear feedback affects the stability of the ecosystem. We summarize our findings in Sec. VIII.

II. MODEL DEFINITIONS

We consider a pool of N species, which we label by $i = 1, \ldots, N$. We write $x_i(t)$ for the abundance of species i in the ecosystem at time t. The dynamics proceed in continuous time, governed by the generalized Lotka-Volterra equations:

$$\dot{x}_i(t) = r_i x_i(t)\left\{K_i - x_i(t) + g\left[\sum_j \alpha_{ij} x_j(t)\right]\right\}. \tag{1}$$

The quantity r_i denotes the growth rate of species i, and K_i is the carrying capacity for the species. In absence of interactions ($\alpha_{ij} = 0$ for all i, j), the abundance x_i can at most take value $x_i = K_i$. In the following we will set $r_i = 1$ and $K_i = 1$ for all species, following Refs. [43,48]. The coefficients α_{ij} describe the interactions between the different species. In the context of random generalized Lotka-Volterra dynamics these are quenched disordered random variables; that is to say, they are chosen from a specified distribution at the beginning, but then remain fixed as the dynamics unfold. We will define the statistics of the α_{ij} below.

The function $g(\cdot)$ describes the "feedback," i.e., how the growth of any one species is affected by the interaction with the other species. We note that Eq. (1) is restricted to functional forms of the type $g(\sum_j \alpha_{ij} x_j)$. In principle, more general forms can be devised, but these are harder to analyze. As we will see below, the model defined in Eq. (1) produces intricate behavior and is sufficient to highlight some of the effects of nonlinear feedback.

Random generalized Lotka-Volterra communities with linear functional feedback, $g(u) = u$, have, for example, been studied in Refs. [24–26,43]. We here focus on nonlinear functions g. We generally assume that g is a nondecreasing function of its argument.

The coefficient α_{ij} denotes the reproductive benefit or detriment species i receives when interacting with species j. We set $\alpha_{ii} = 0$; self-interaction is already accounted for in Eq. (1). In our model we assume that the off-diagonal coefficients are drawn from a Gaussian distribution with the following statistics:

$$\overline{\alpha_{ij}} = \frac{\mu}{N},$$
$$\overline{\alpha_{ij}^2} - \frac{\mu^2}{N^2} = \frac{\sigma^2}{N}. \tag{2}$$

Inline with literature on disordered systems [18] we use an overbar to indicate the average over the quenched random variables $\{\alpha_{ij}\}$. Equations (2) indicate that the mean of each matrix element is μ/N, and their variance is σ^2/N. The scaling with N is standard in the context of disordered systems, and is chosen to guarantee a meaningful thermodynamic limit $N \to \infty$, which we will eventually assume in the generating-functional analysis.

The parameter μ controls the "baseline" interaction between any pair of species. Negative values of μ indicate a generally competitive environment; the presence of any species leads to negative feedback on the growth of the other species. Similarly, if μ takes positive values, then species generally interact positively with each other, and the presence of one species tends to enhance the growth of all other species. One expects this to potentially lead to unlimited growth as in Refs. [24,25], at least in the absence of saturation effects in the nonlinear feedback. We will refer to μ as the cooperation parameter. This is also known as the competition–mutualism parameter in ecology [49].

The parameter σ describes the degree of heterogeneity in the interaction of species, we will call it the "heterogeneity parameter." We also allow for correlations between the interaction coefficients α_{ij} and α_{ji} for any pair $i \neq j$ of species. Specifically, we write these as follows:

$$\overline{\alpha_{ij}\alpha_{ji}} - \frac{\mu^2}{N^2} = \gamma\frac{\sigma^2}{N}, \tag{3}$$

where the model parameter γ can take values between -1 and 1. The role of γ can best be understood by considering the case $\mu = 0$. In this case, $\overline{\alpha_{ij}\alpha_{ji}} = \gamma\sigma^2/N$. For $\gamma = -1$ one then finds $\alpha_{ij} = -\alpha_{ij}$ with probability one, i.e., species form predator-prey pairs; one species in each pair benefits from the presence of the other, but that other species is adversely affected by the presence of the first. For $\gamma = 0$ (and still assuming $\mu = 0$) the interaction coefficients α_{ij} and α_{ji} are uncorrelated, i.e., half of all pairs of species will be of the predator-prey type, and the other half will either both benefit from each other, or each be suppressed by the presence of the other species. For $\gamma = 1$ finally, there are no predator-prey pairs. Instead, $\alpha_{ij} = \alpha_{ji}$ with probability one, i.e., both species i and j profit from each other's presence, or the interaction is negative in both directions. If $\mu \neq 0$, then the combination of α_{ij}, α_{ji} is drawn from a bivariate Gaussian distribution with nonzero mean, and the number of competitive, cooperative, and exploitative interactions can be obtained from the probabilities in the different quadrants of the α_{ij}-α_{ji} plane. We will call γ the symmetry parameter.

The main objective of our work is to investigate how the parameters μ, σ, and γ affect the outcome of the generalized Lotka-Volterra dynamics in the presence of nonlinear feedback.

III. NUMERICAL RESULTS FOR NONLINEAR FEEDBACK

We first focus on a model similar to Holling type-II functional response [50,51]. This form of feedback was originally introduced to model the rate of growth of a predator while interacting with prey; it is natural that the benefit from additional prey will eventually saturate when prey numbers are large. We extend the idea of a saturating function to all types of inter-species interactions, and study the following feedback function,

$$g(u) = g_H(u) \equiv \frac{2au}{a + 2|u|}. \tag{4}$$

The subscript H stands for Hill function. This function has a sigmoidal shape and saturates to $g_H = a$ for $u \gg 1$ and to $g_H = -a$ for $u \ll -1$. We note that $g_H(u = \pm a/2) = \pm a/2$, i.e., the half-point of saturation is reached at $u = \pm a/2$. More general forms of the Hill function can be considered, but we here restrict the analysis to the form in Eq. (4), with one single parameter a.

In numerical simulations of the generalized Lotka-Volterra system with this type of feedback we broadly find three different dynamical outcomes: In some cases the system converges

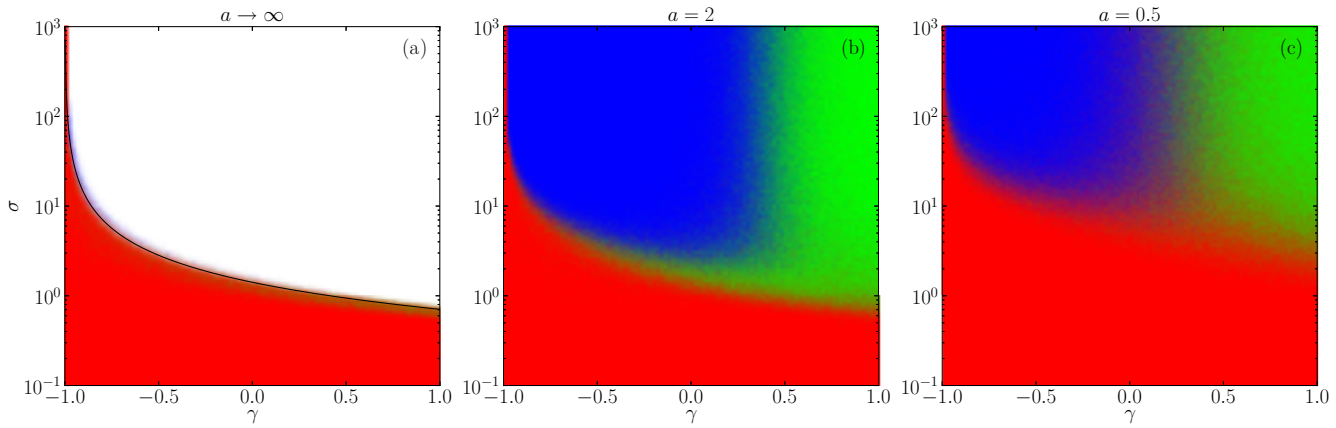

FIG. 1. Phase diagram obtained from simulations of the generalized Lotka-Volterra system with $N = 200$. Panel (a) shows the case $a \to \infty$ (i.e., linear feedback), panels (b) and (c) are for nonlinear feedback, with $a = 2$ in (b), and $a = 0.5$ in (c). Simulations are for $\mu = 0$. The colors indicate the dominant outcome in each part of parameter space, with red (medium gray) representing a unique stable fixed point, green (light gray) multiple fixed points, blue (dark gray) indicating parameters for which the dynamics do not converge, and white indicating unbounded growth of species abundances. The solid line in panel (a) describes the onset of instability as derived from theory (see Refs. [24,25,43]).

to a unique fixed point. That is to say, for a fixed draw of the interaction matrix elements $\{\alpha_{ij}\}$ the dynamics converge to one single fixed point, independent of what initial conditions are used for the $\{x_i\}$. In other cases we also find fixed points, but these are no longer unique. That is, while runs are generally found to converge, the system has multiple marginally stable fixed-point attractors, and which one is eventually reached depends on the initial condition. The third type of outcome we find is one in which the dynamics never settles down and remains volatile until the end of the simulation. The general types of behavior have been found previously in related systems, for example, in random replicator systems, and in models of game learning [17,33,45].

For $a \to \infty$ we recover unrestricted linear feedback; the system can then display a fourth type of behavior: unbounded growth [24,25,43]. This is due to the lack of saturation. The absence of unlimited growth for finite values of the saturation parameter a can directly be inferred from Eq. (1). For $r_i = K_i = 1$ the relative growth rate of species i is given by $\dot{x}_i/x_i = (1 - x_i + g_i)$, where $g_i = g_H(\sum_j \alpha_{ij} x_j)$ at most takes value $g_i = a$. Thus, the abundance of any species, x_i, is limited to at most $x_i = 1 + a$, as the growth rate for species i then reduces to zero. We note the difference with random replicator dynamics [17,21,33], in which the total abundance is constant in time ($N^{-1} \sum_i x_i = 1$) by construction, but where none of the single variables x_i is constrained to a fixed interval in the thermodynamic limit.

We present numerical simulations for the generalized Lotka-Volterra system with nonlinear feedback in Fig. 1. The figures illustrates the behavior of the system in the plane spanned by the symmetry parameter γ and the heterogeneity parameter σ, for different values of the saturation parameter a. For each combination of these parameters we have carried out an ensemble of runs of the dynamics, and have recorded how frequently each dynamic outcome is observed. We describe how we distinguish between the three types of behavior in the Supplemental Material [52]. The frequencies with which the different outcomes are found are then converted into a color (grayscale) code. Red coloring (medium gray) in the figure indicates parameters for which convergence to unique fixed points is found. In the green (light gray) areas of the phase diagram, we also observe predominantly convergence to fixed points, but the system has multiple such attractors, and which one is reached depends on the initial condition. In the blue (dark gray) areas of the graphs finally we find volatile behavior, the trajectories generated by the generalized Lotka-Volterra system do not settle down by the end of our simulations.

We broadly find the following phase behavior. For sufficiently small heterogeneity σ the system is stable and has a unique fixed point. This region of stability tends to be larger for low values of the symmetry parameter γ than for higher values. The presence of predator-prey pairs (anticorrelation of the matrix elements) thus promotes the existence of a unique stable fixed point, inline with previous observations, for example, in Refs. [25,43]. If the heterogeneity σ exceeds a critical value σ_c, then the system either enters a phase with multiple stable fixed points or it fails to converge. The latter tends to happen for lower values of γ, i.e., anticorrelated or moderately correlated interactions, the former for higher values of γ, when the interactions are increasingly correlated. The data in the figure shows that the saturation of the nonlinear feedback stabilizes the dynamics, with the globally stable region becoming larger for smaller values of the saturation parameter a (i.e., for stronger nonlinearity). For $a = \infty$ [Fig. 1(a)] we recover the unrestricted generalized Lotka-Volterra system with linear feedback, for which σ_c^2 is analytically known to be $\sigma_c^2 = 2/(1 + \gamma)^2$ [24–26,43]. This boundary is shown in Fig. 1(a) as a solid line. For this particular choice of parameters the system shows unlimited growth in the unstable phase [indicated in Fig. 1(a) by the absence of background shading].

We note that not all samples of the system show the same behavior for any given set of parameters. For example, some runs may converge and others may fail to settle down before the end of the simulation. We believe that this is due to the finite number of species, finite integration time-step, and finite run-time required in simulations, and we would expect the

boundaries to become more sharp in the asymptotic limit and for infinitely large systems. We also see trajectories which remain seemingly chaotic for a long time and then reach a fixed point only at very long times. The phase diagram in Fig. 1 shows the typical behavior. Technically, we cannot exclude heteroclinic cycles based on our simulations, however we have not witnessed any such behavior before the end-time of our numerical integration. In some regions of parameter space (most notably near the phase line), we also find that the number of simulations runs displaying a unique fixed point reduces when we increase the number of species N.

IV. GENERATING FUNCTIONAL ANALYSIS

A. Generating functional

The generating-functional analysis proceeds along the lines of Refs. [17,33]. Starting from the dynamics in Eq. (1) one introduces the generating functional as

$$Z[\boldsymbol{\psi}] = \left\langle e^{i\sum_i \int dt\ x_i(t)\psi_i(t)} \right\rangle, \tag{5}$$

where $\langle \ldots \rangle$ denotes an average over paths of the process; this includes averaging over potentially random initial conditions (we assume that the distributions of these are independent and identical across species). The field $\boldsymbol{\psi}$ is a source term. In essence $Z[\boldsymbol{\psi}]$ is the Fourier transform of the probability measure in the space of paths of the generalized Lotka-Volterra system. The generating functional is subsequently averaged over the quenched random coupling matrix, and the thermodynamic limit, $N \to \infty$ is taken. These steps are well-established, and the calculation is lengthy. We therefore only quote the final result here. Further intermediate steps are reported in the Supplemental Material [52].

B. Effective representative species process

The final outcome of the path-integral analysis, after the disorder has been averaged out and the thermodynamic limit has been taken, is an effective "mean-field" process for a single representative species. For the case of the generalized Lotka-Volterra dynamics in Eq. (1) (with $r_i = 1, K_i = 1$) the effective process is of the form

$$\dot{x}(t) = x(t)\Big\{1 - x(t) + g\Big[\mu M(t) + \gamma\sigma^2 \int_0^t dt'\ G(t,t')x(t') + \eta(t)\Big]\Big\}, \tag{6}$$

where one has the following self-consistent relations

$$\begin{aligned} M(t) &= \langle x(t)\rangle_*, \\ \langle \eta(t)\eta(t')\rangle &= \sigma^2\langle x(t)x(t')\rangle_*, \\ G(t,t') &= \left\langle \frac{\partial x(t)}{\partial \eta(t')} \right\rangle_*. \end{aligned} \tag{7}$$

In these equations $\langle \cdots \rangle_*$ denotes the average over realizations of the effective process, i.e., over the noise $\eta(t)$ and potentially random initial conditions. We will refer to $M(t)$, the correlation function $C(t,t') = \langle x(t)x(t')\rangle_*$, and the response function $G(t,t')$ as the macroscopic dynamical order parameters. In the context of ecology $M(t)$ is a measure of the average abundance in the system per species.

We note that the description in terms of the above effective process is also known as "dynamical mean-field theory." The process can alternatively be obtained using the cavity method, for models with linear feedback this is discussed in Refs. [24–26,39,48,53].

C. Fixed-point analysis

We proceed to evaluate fixed points of the effective dynamics in Eq. (6). The corresponding fixed-point relations are

$$x^*[1 - x^* + g(\mu M^* + \gamma\sigma^2\chi x^* + \eta^*)] = 0, \tag{8}$$

where we have used the superscript * to indicate quantities evaluated at the fixed point. In the fixed-point regime one has $G(t,t') = G(t-t')$ (time-translation invariance), and we have introduced the integrated response $\chi = \int_0^\infty d\tau\ G(\tau)$. The correlation function $C(t,t') = \langle x(t)x(t')\rangle_*$ becomes independent of t and t' at the fixed point, and we write $q \equiv C(t,t')$. We can then replace η^* by $\eta^* = \sigma\sqrt{q}z$, where z is a static Gaussian random variable of mean zero and with variance one.

Equation (8) always has the solution $x^*(z) = 0$ for all z. Potential other solutions fulfill the relation

$$x^* = 1 + g(\mu M^* + \gamma\sigma^2\chi x^* + \sigma\sqrt{q}z). \tag{9}$$

Such solutions are only physically valid provided they are nonnegative, as x^* describes the abundance of an effective species.

It is difficult to proceed analytically for general choices of the function g. In particular, if g is nonlinear, then Eq. (9) would have to be solved numerically for $x^*(z)$ for a given value of z. We therefore consider a piecewise linear feedback function g. Specifically, we follow Ref. [53] and approximate the nonlinear feedback by

$$g(u) = g_P(u) = \begin{cases} a & u \geqslant a, \\ u & -a \leqslant u \leqslant a, \\ -a & u \leqslant -a. \end{cases} \tag{10}$$

The subscript g_P refers to piecewise linear. This function is linear in u in the interval $-a \leqslant u \leqslant a$, and is then "clipped." Similar to the nonlinear feedback the function saturates at a for large u, and at $-a$ for large negative values of u. We also note that $g(a/2) = a/2$, i.e., the saturation half-point of the piecewise linear model is the same as for the nonlinear feedback in Eq. (4). This structure allows us to proceed with the mathematical analysis, and at the same time it conserves some of the main features of the Holling type-II system as we will discuss further below.

To find the solution $x^*(z)$ of Eq. (9) we consider the three branches of $g_P(u)$. These are separated by threshold values z_1 and z_2 for the static noise variable z; we will evaluate these thresholds below. Specifically, we find

(i) For $z \geqslant z_2$, the argument of the function g_P exceeds a and hence $g_P(u) = a$; this gives the solution $x^*(z) = 1 + a$;

(ii) For $z_1 \leqslant z \leqslant z_2$ one has $g_P(u) = u$, giving $x^*(z) = \frac{1+\mu M^* + \sigma\sqrt{q}z}{1-\gamma\sigma^2\chi}$;

(iii) For $z \leqslant z_1$ finally, the value $x^*(z)$ depends on the choice of the saturation parameter a in the following way: If

a is smaller than the carrying capacity (i.e., $a \leqslant 1$), then the feedback saturates at $g_P = -a$, and we find $x^*(z) = 1 - a$. If $a \geqslant 1$, then the (effective) species dies out, $x^*(z) = 0$, before the feedback reaches saturation.

The threshold values z_1 and z_2 are found from the argument of the function g in Eq. (9):

$$z_1 = \frac{(1-a)(1-\gamma\sigma^2\chi)\Theta(1-a) - (1+\mu M^*)}{\sigma\sqrt{q}},$$
$$z_2 = \frac{(1+a)(1-\gamma\sigma^2\chi) - (1+\mu M^*)}{\sigma\sqrt{q}}. \tag{11}$$

In the first expression $\Theta(\cdot)$ is the Heaviside step function, used here to differentiate between the cases $a \geqslant 1$ and $a \leqslant 1$. A more detailed discussion can be found in Sec. S1 H of the Supplemental Material [52].

Putting the different cases together we find the following physical fixed-point value for a given combination of z and a,

$$x^*(z) = \begin{cases} 1+a & z \geqslant z_2, \\ \frac{1+\mu M^* + \sigma\sqrt{q}z}{1-\gamma\sigma^2\chi} & z_1 \leqslant z \leqslant z_2, \\ (1-a)\Theta(1-a) & z \leqslant z_1. \end{cases} \tag{12}$$

We note that the abundance x^* of the effective species is bounded from above by $1 + a$. This indicates that, unlike in standard generalized Lotka-Volterra dynamics, abundances cannot diverge, and hence the average species population given by the order parameter M^* also remains finite. The lower bound for the solutions of Eq. (9) is zero for $a \geqslant 1$, and given by $1 - a$ for $a \leqslant 1$.

It is important to recall that $x^*(z) = 0$ is a solution of the fixed-point Eq. (8) for all z. However, we find in linear stability analysis that this zero solution is an attractor only when $a \geqslant 1$ and $z \leqslant z_1 = -\frac{1+\mu M^*}{\sigma\sqrt{q}}$, i.e., only when $x^*(z) = 0$ is the unique solution of the fixed point Eq. (8). This is shown in Sec. S1 I of the Supplemental Material [52]. For $a < 1$, the solution $x^* = 0$ cannot be realizd, and all species in the initial pool will have nonzero abundances in the phase of unique stable fixed points.

Using Eq. (12) we can write Eqs. (7) in the following form:

$$M^* = \int_{z_2}^{\infty}(a+1)Dz + \int_{z_1}^{z_2}\frac{1+\mu M^* + \sigma\sqrt{q}z}{1-\gamma\sigma^2\chi}Dz + \Theta(1-a)\int_{-\infty}^{z_1}(1-a)Dz, \tag{13a}$$

$$q = \int_{z_2}^{\infty}(a+1)^2Dz + \int_{z_1}^{z_2}\left(\frac{1+\mu M^* + \sigma\sqrt{q}z}{1-\gamma\sigma^2\chi}\right)^2 Dz + \Theta(1-a)\int_{-\infty}^{z_1}(1-a)^2Dz, \tag{13b}$$

$$\chi = \frac{1}{1-\gamma\sigma^2\chi}\int_{z_1}^{z_2}Dz, \tag{13c}$$

where we have introduced the shorthand $Dz = \frac{dz}{\sqrt{2\pi}}e^{-z^2/2}$ for the Gaussian measure of z. The quantity M represents the mean species abundance, q is the second moment of the species-abundance distribution, and χ is a "susceptibility," capturing how the fixed-point values of the species abundances shift in response to persistent perturbations.

Together with Eqs. (11) this is a self-consistent set of relations for the order parameters q, χ, and M^* in the regime of unique stable fixed points. Solutions of these equations can be obtained numerically as function of the model parameters μ, σ, γ, and a. The method we use to solve this set of equations is described in the Sec. S3 of the Supplemental Material [52].

D. Linear stability analysis

We now carry out a linear stability analysis of the fixed points identified in the previous section. We first notice that fixed points of the form $x^*(z) = 1 + a, x^*(z) = (1 - a)\Theta(1 - a)$ are always locally stable. This is shown in Section S1 I in the Supplemental Material [52].

We note that the function $g(\cdot)$ is the identity function in the vicinity of the remaining fixed points. We write $x(t) = x^* + y(t)$ and $\eta(t) = \sigma\sqrt{q}z + v(t)$, and following Ref. [21] we add noise of zero mean and unit amplitude $\xi(t)$ in the effective process to study stability.

Linearizing the effective dynamics in Eq. (6) in y and v we find

$$\dot{y}(t) = x^*\left[-y(t) + \gamma\sigma^2\int_0^t dt' G(t-t')y(t') + v(t) + \xi(t)\right]. \tag{14}$$

Carrying out a Fourier transform, this can be written as

$$\frac{i\omega\tilde{y}(\omega)}{x^*} = [\gamma\sigma^2\tilde{G}(\omega) - 1]\tilde{y}(\omega) + \tilde{v}(\omega) + \tilde{\xi}(\omega). \tag{15}$$

Following Refs. [17,33] we now focus on the long-time behavior of perturbations, i.e., on the mode at $\omega = 0$. This allows one to identify the transition to instability found in simulations, as described in more detail below. Broadly speaking, the behavior of the $\omega = 0$ mode is related to the long-term decay of perturbations. Discussions of stability conditions and the relevance of $\omega = 0$-modes can also be found in Refs. [32,39]. Rearranging Eq. (15) and taking averages we find

$$\langle|\tilde{y}(0)|^2\rangle = \phi\frac{\langle|\tilde{v}(0)|^2\rangle + 1}{(1-\gamma\sigma^2\chi)^2}, \tag{16}$$

where the factor $\phi = \int_{z_1}^{z_2}Dz$ accounts for the fact that Eq. (14) only applies to fixed points for which g is not saturated, i.e., for values of z with $z_1 \leqslant z \leqslant z_2$. Finally, using the self-consistency relation $\langle|\tilde{y}(0)|^2\rangle = \sigma^2\langle|\tilde{v}(0)|^2\rangle$, we find

$$\langle|\tilde{y}(0)|^2\rangle = \frac{\phi}{(1-\gamma\sigma^2\chi)^2 - \phi\sigma^2}. \tag{17}$$

This quantity is finite (and nonnegative) in the phase of stable fixed points and becomes infinite when

$$\phi = \frac{(1-\gamma\sigma^2\chi)^2}{\sigma^2}. \tag{18}$$

This condition signals the onset of instability. Analogous conditions for Lotka-Volterra models with linear feedback have been related to stability conditions derived from random-matrix approaches; see, for example, Refs. [17,39,43] for

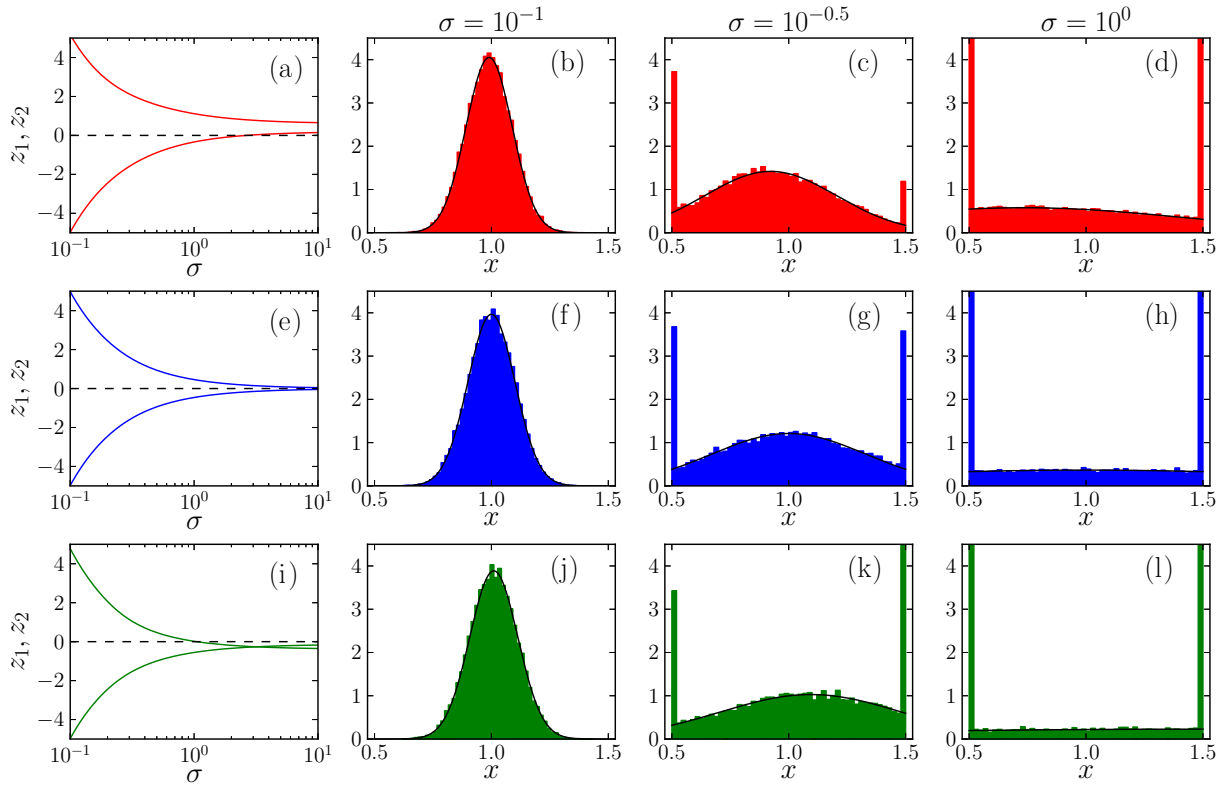

FIG. 2. Species abundance distribution for the case $a = 0.5$ and $\mu = 0$ for different values of the heterogeneity parameter σ. The upper row [panels (a–d)] is for $\gamma = -1$, the middle row [(e–h)] for $\gamma = 0$, and the lower row [panels (i–l)] for $\gamma = 1$. On the left [panels (a, e, i)] we show z_2 (upper line) and z_1 (lower line), remaining panels show the species abundance distributions, for $\sigma = 10^{-1}$ [panels (b, f, j)], $\sigma = 10^{-0.5}$ [panels (c, g, k)], and $\sigma = 1$ [panels (d, h, l)]. Solid lines are theoretical predictions for the species abundance distribution, shaded histograms are from simulations.

further discussion. This is related to what is known as "structural instability" in ecology; see Refs. [16,42].

V. TEST AGAINST SIMULATIONS AND PHASE DIAGRAM

A. Species abundance distributions

We first discuss the resulting species abundance distributions in the regime of unique stable fixed points (i.e., the distribution of the $\{x_i\}$). In Fig. 2 we show examples of species abundance distributions for different values of σ and γ for $a = 0.5$ and $\mu = 0$. The shaded histograms in the figures are from simulations, solid black lines indicate the distributions of the unsaturated species from the theory. On the left of each of the figure [Figs. 2(a), 2(e) and 2(i)] we show how z_2 (upper line) and z_1 (lower line) vary with increasing heterogeneity σ.

To interpret the histograms in Fig. 2 we note that the weight of each branch of the solution in Eq. (12) is equal to the probability of a standard Gaussian random number z to fall between or on either side of z_1 and z_2, respectively. For $\sigma = 0$, there is no species heterogeneity ($\alpha_{ij} = 0$ for all i, j); all species abundances take the value $x^* = M^*$, where $M^* = 1/(1-\mu)$ from Eq. (13a). One finds $z_1 \to -\infty$ and $z_2 \to \infty$, and the nonlinear feedback does not reach saturation.

For nonzero values of the interaction heterogeneity σ, z_1, and z_2 become finite; as a consequence there is a finite probability of z falling outside the interval $[z_1, z_2]$, and hence the nonlinear feedback saturates for a finite fraction of species. This results in a clipped Gaussian distribution for x^*; the fraction of species in the clipped regions increases with σ.

We find that both z_1 and z_2 are decreasing functions of γ, this is consistent with Eqs. (11), where the explicit factor of γ dominates over the dependence of M^*, q and χ on γ. As a consequence the proportion of species "clipped off" at either side changes as γ varies. We find a lower mean species abundance M^*, and more species at $1-a$ than at $1+a$ for $\gamma = -1$, and a higher mean abundance with more species at the upper bound $1+a$ for $\gamma = 1$.

We find similar results for $a = 2$; these are shown in Fig. S1 in the Supplemental Material [52]. As the limiting values ($x^* = 0$ and $x^* = 1+a$) for the species abundances are further apart for this case, a higher value of σ is required to spread the abundance distribution to these values. Therefore we find less saturation for $a = 2$ than for $a = 0.5$ at a fixed value of the heterogeneity parameter σ.

B. Test of theoretical predictions for order parameters in the phase of unique stable fixed points

The analytical theory results in predictions for the order parameters q, χ, and M^* as a function of the model parameters a, μ, γ, and σ. These predictions are obtained as the solutions of the coupled Eqs. (13a), (13b), and (13c). They are valid in the parameter regime in which the generalized Lotka-Volterra

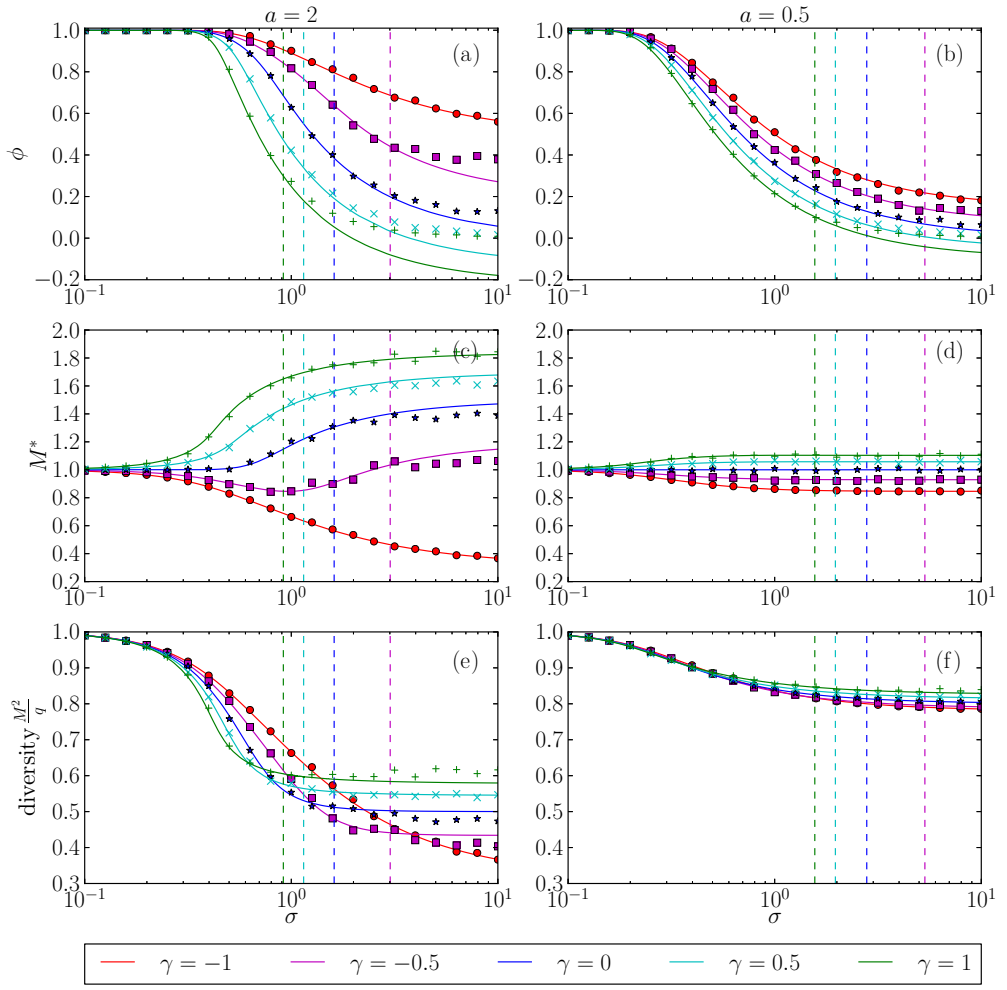

FIG. 3. Comparison of theoretical predictions (lines) for the characteristic order parameters against simulations (markers). Data is for $\mu = 0$, $\gamma = -1$ (•), -0.5 (■), 0 (★), 0.5 (×), and $\gamma = 1$ (+). This is for the model with piecewise linear feedback. Left-hand column [panels (a, c, e)] is for $a = 2$, right-hand column [panels (b, d, f)] for $a = 0.5$. The vertical dashed lines mark the onset of instability as predicted by the theory; analytical predictions can no longer be expected to match with simulations in the phase to the right of the dashed lines. The graphs show the fraction of species not saturated ϕ, the mean abundance M^*, and the diversity M^2/q as functions of σ.

system converges to a unique stable fixed point, independent of initial conditions.

A comparison of theory and simulation is shown in Fig. 3. Theoretical predictions are indicated by solid lines, results from simulations as symbols. We show the quantities ϕ, M^* and a measure of diversity related to Simpson's index. Simpson's index [54] is the probability that two randomly chosen individuals in the community are of the same species, $\mathcal{S} = \sum_i (\frac{x_i}{\sum_j x_j})^2$. For our model this index is given by $\mathcal{S} = q/(NM^2)$. A low value of this probability indicates high diversity of species; therefore the inverse Simpson index, $\mathcal{S}^{-1} = NM^2/q$ characterizes the diversity of the ecological community. The diversity scales linearly with N; therefore, we report the relative diversity $\mathcal{S}^{-1}/N = M^2/q$. A more detailed explanation of how these quantities were measured from simulations and predicted from the theory can be found in Section S2 of the Supplemental Material [52].

The vertical dashed lines in Fig. 3 indicate the predicted onset of instability. More precisely unique stable fixed points are predicted for small values of σ, i.e., to the left of the dashed lines. To the right of these lines the system either has multiple fixed points, or never settles down, and in either of these scenarios the analytical predictions for the stable fixed point phase can no longer be expected to apply. The figure indicates agreement between theory and simulation in the stable phase. Systematic deviations can be found in the unstable regime, although the predictions from the theory appear to remain a good approximation in some cases. Similar observations have been made in related models, see e.g., [25,33]. We note that solving Eqs. (13) can lead to $z_1 > z_2$ in the unstable phase. This results in the prediction of a negative value of ϕ (the fraction of unsaturated species), which demonstrates further that the theory does not apply in this parameter regime.

The mean abundance, M^*, tends to higher values for positive values of the symmetry parameter γ, i.e., in absence of exploitative interactions and predator-prey pairs. This is shown in Figs. 3(c) and 3(d). This can be understood from the species abundance distributions in Fig. 2 and from the dependence

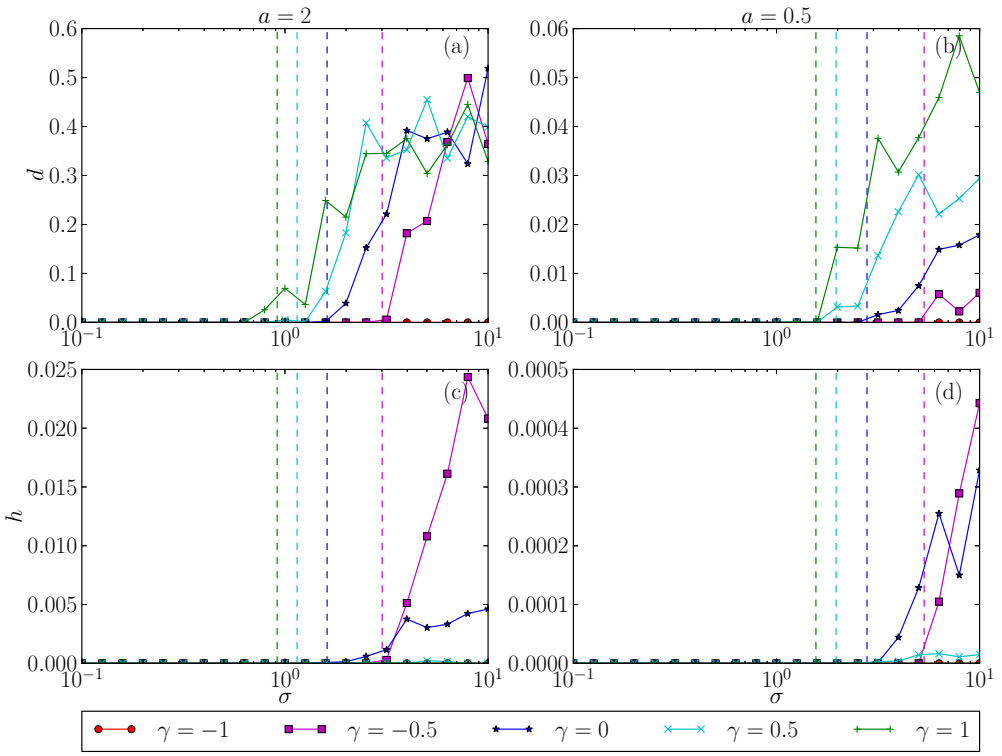

FIG. 4. Onset of instability for the model with piecewise linear feedback. Left-hand column [panels (a, c)] is for $a = 2$, right-hand column [panels (b, d)] for $a = 0.5$. The vertical dashed lines mark the onset of instability as predicted by the theory. The graphs show d (top) and h (bottom). Data is for $\mu = 0$, and $\gamma = -1(\bullet), -0.5(\blacksquare), 0(\bigstar), 0.5(\times), 1(+)$.

of this distribution on γ. We find more species with larger abundances for positive γ, and more species with smaller abundances for negative γ. This is due to the dependence of z_1 and z_2 on γ as discussed in Sec. V A. These effects are reduced for stronger nonlinearity, as shown in Fig. 3(d). Generally, we find that a lower value of the saturation parameter a reduces the dependence of the order parameters on γ. We also note that a much higher diversity of species is maintained for a lower saturation value [cf. Figs. 3(e) and 3(f)].

C. Onset of instability

In Fig. 4 we investigate the onset of instability in more detail. We use several indicators to detect different types of behavior in the numerical solutions of the generalized Lotka-Volterra equations. To characterize the (relative) variation of species abundances over time, we calculate

$$h = \frac{\left\langle \langle x_i(t)^2 \rangle_T - \langle x_i(t) \rangle_T^2 \right\rangle_N}{\left\langle \langle x_i(t) \rangle_T^2 \right\rangle_N}. \tag{19}$$

In this expression, $\langle \cdots \rangle_T$ indicates an average over time; this is taken in the stationary state; reported values are time averages over the last 1% of trajectories (numerical integration of the generalized Lotka-Volterra equations is carried out up to final time $T_f = 200$). The notation $\langle \ldots \rangle_N$ in Eq. (19) denotes an average over species, $\langle \ldots \rangle_N = N^{-1} \sum_i \cdots$. The order parameter h indicates whether or not the system settles down to a fixed point: when $h = 0$ a fixed point is reached eventually, whereas positive values of h indicate persistent volatile dynamics. To identify the phase with multiple fixed points, we have additionally run the following numerical experiments. For a fixed realization of the interaction matrix we have generated two independent random initial conditions. We then run each of these separately and compute the relative distance

$$d = \frac{\langle \langle (x_i(t) - x_i'(t))^2 \rangle_N \rangle_T}{\left\langle \langle x_i(t) \rangle_N^2 \right\rangle_T}, \tag{20}$$

where x_i and x_i' are the trajectories for the two sets of initial conditions. This quantity is again evaluated in the stationary state. Thus, $d \approx 0$ when the asymptotic behavior is independent of initial conditions, and $d > 0$ otherwise.

The data shown in the upper panels of Fig. 4 shows that $d \approx 0$ for small heterogeneity σ independently of the symmetry parameter γ, but that a phase with dependence on initial conditions is found when the stability threshold is crossed ($\sigma > \sigma_c$). The results in the lower panels of Fig. 4 indicate that the dynamics remains volatile ($h > 0$) for large values of σ when the symmetry parameter is zero or moderately negative. The figure shows that a fixed point is almost certainly reached for $\gamma = 1$ and is likely to be reached for $\gamma = 0.5$, although these fixed points are not unique.

Comparing the scales of the left- and right-hand panels in Fig. 4 shows that the order parameters d and h are much smaller for the lower value of the saturation a; this is due to the tighter bounding effect of the nonlinear feedback.

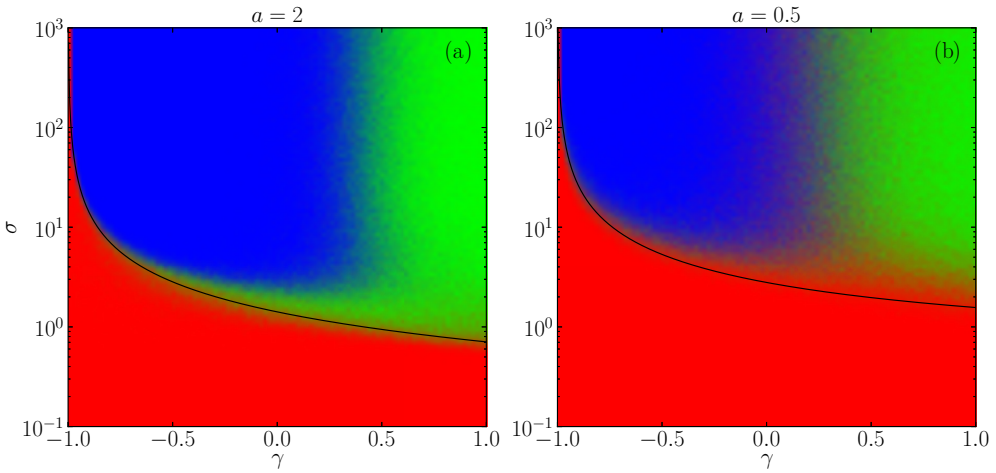

FIG. 5. Phase diagram obtained from simulations of the generalized Lotka-Volterra systems with piecewise linear feedback with $N = 200$. As in Fig. 1 the colors (gray shading) indicate the dominant outcome in each part of parameter space [red (medium gray): unique stable fixed point; green (light gray): multiple fixed points; blue (dark gray): dynamics do not converge]. Solid black lines show the onset of instability as predicted from the generating-functional approach. Data is for $\mu = 0$, panel (a) for $a = 2$, panel (b) for $a = 0.5$.

VI. COMPARISON OF generalized LOTKA-VOLTERRA SYSTEMS WITH NONLINEAR AND PIECEWISE LINEAR FEEDBACK

A. Phase diagram and onset of instability

In Fig. 5 we show examples of the phase diagram obtained from numerical integration of the generalized Lotka-Volterra system with piecewise linear response. These are generated in the same way as in Fig. 1. Red (medium gray) indicates parameter values of the phase with unique fixed points, green (light gray) indicates multiple fixed points, and blue (dark gray) indicates volatile behavior. The black line in each panel shows the boundary, σ_c, of the phase with a unique stable fixed point, predicted by the theory. As seen in the figure the theory is in agreement with results from numerical integration of the generalized Lotka-Volterra system. We attribute remaining minor discrepancies to finite integration time, finite time steps, and finite species number.

Comparing Figs. 1 and 5, we find that the behavior of the systems with nonlinear and piecewise linear feedback are very similar. Unique fixed points are reached for values of σ below a critical point for all values of the symmetry parameter γ, with much higher critical values σ_c for lower γ. This indicates higher stability for asymmetric couplings than in the symmetric case. Above this critical value of the heterogeneity parameter we find multiple fixed points for positively correlated interactions, and persistent volatile behavior, such as limit cycles, chaos, or potentially heteroclinic cycles for negatively correlated couplings. In Figs. 1 and 5, one notices the stabilizing effect of a lower value of the saturation parameter a in the nonlinear feedback, i.e., for smaller a one finds a larger red (medium gray) area indicating stable unique fixed points, and higher critical values for σ.

We have observed that the area of unique fixed points in the phase diagrams becomes bigger for smaller values of the number of species N. Conversely, we would expect the results from simulations to converge to the analytical prediction in Fig. 5(b) for higher values of N. Interestingly, this effect is more pronounced for $a = 0.5$ than for $a = 2$. That is, for $a = 0.5$ the system retains more structural stability as N is increased than for $a = 2$. This underlines the stabilizing effect of the nonlinear feedback.

To make the comparison between the two models more precise we report results for the order parameters h and d from numerical simulations of the model with nonlinear feedback in Fig. 6, along the analytical prediction for the onset of instability in the model with piecewise linear response. The data shows that the system with nonlinear feedback has very similar behavior as that with the piecewise linear feedback. We find volatile dynamics for anticorrelated interactions past the critical interaction heterogeneity, and multiple fixed points for correlated interactions. The point at which h and d become nonzero is very close to the onset of instability predicted by the theory for the model with piecewise linear feedback.

B. Order parameters in the stable phase

In Fig. 7 we compare results from numerical integration of the generalized Lotka-Volterra equations with nonlinear feedback (markers), with the analytical solutions for piecewise linear feedback (lines). As seen in the figure the general behavior of the mean abundance M^* and diversity as functions of σ and γ are similar in both models.

The main difference between the piecewise linear function and the nonlinear function is how they approach their upper and lower limits $\pm a$. The piecewise linear function $g_P(u)$ approaches its limits linearly, and attains them at $u = \pm a$ [$g_P(\pm a) = \pm a$]; the nonlinear Hill function g_H approaches the limits much more slowly, and only attains them asymptotically. As a consequence, we have $|g_H(u)| < |g_P(u)|$ for $|u| > a/2$. The differences in the two functions account for the differences we see between the results in Fig. 7. We find the order parameters M^* and diversity to display a much smoother dependence on heterogeneity for the nonlinear function (markers) than for the piecewise function.

For the larger values of σ shown in Fig. 7(a), we find that M^* is lower for the nonlinear function for all values of γ. For $a = 2$ species die before they can saturate to the lower

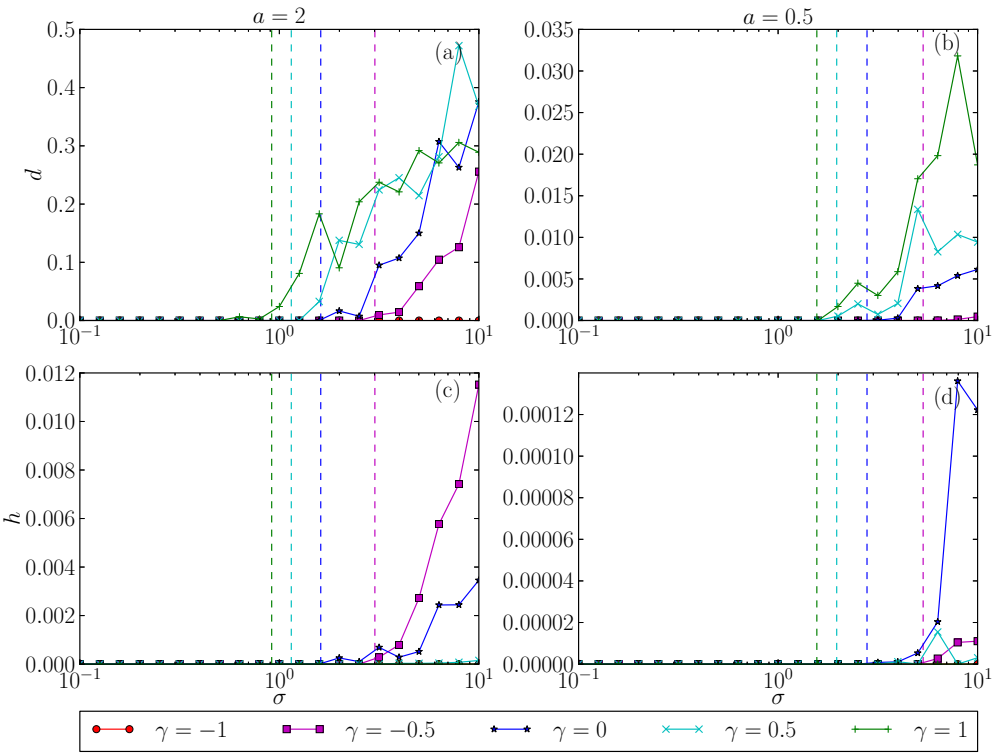

FIG. 6. Onset of instability for nonlinear feedback. Left-hand column [panels (a, c)] is for $a = 2$, right-hand column [panels (b, d)] for $a = 0.5$. The vertical dashed lines mark the onset of instability predicted for the piecewise feedback function from theory. The graphs show d (top) and h (bottom). Data is for $\mu = 0$, $\gamma = -1(\bullet), -0.5(\blacksquare), 0(\bigstar), 0.5(\times), 1(+)$.

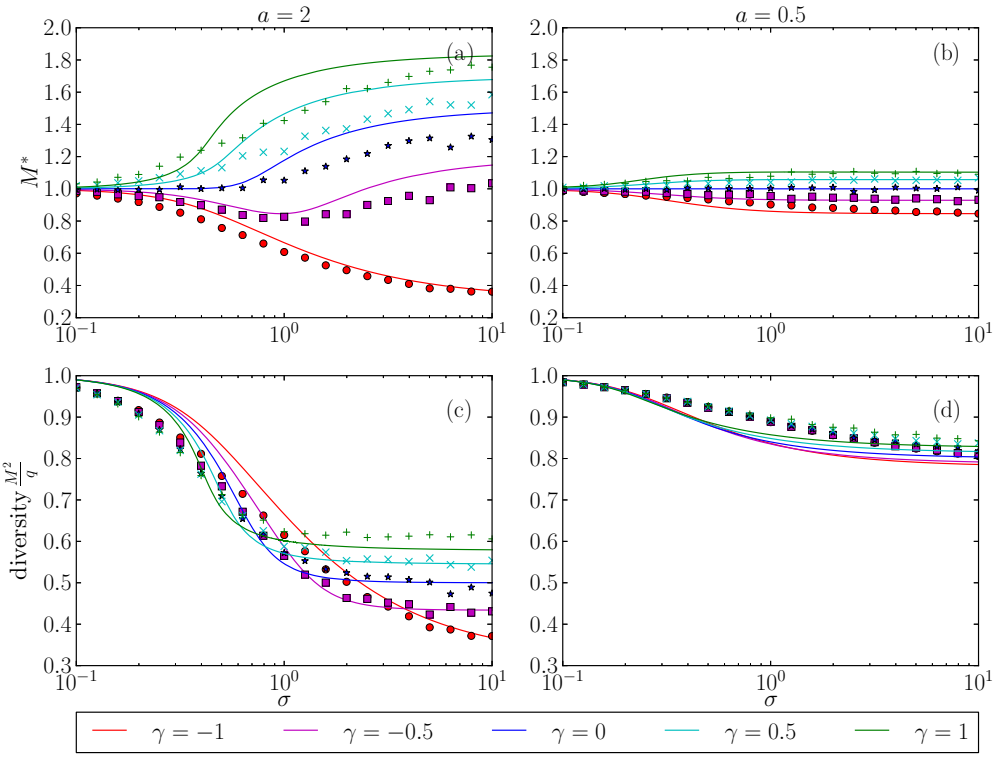

FIG. 7. Comparison of theoretical predictions for M^* and diversity for the piecewise feedback (lines) against simulations for nonlinear feedback (markers). Left-hand column [panels (a, c)] is for $a = 2$, right-hand column [panels (b, d)] for $a = 0.5$. Data is for $\mu = 0$, $\gamma = -1(\bullet), -0.5(\blacksquare), 0(\bigstar), 0.5(\times), 1(+)$.

boundary. In this case the difference in saturation is therefore only present at the upper limit, and this results in lower values of M^* for the nonlinear function. This is because species are closer to upper saturation point for higher values of σ, where the nonlinear function is lower in magnitude than the piecewise linear function. The lower value of the nonlinear function causes these species to have lower abundances than in the piecewise case.

For $a = 0.5$, species are able to reach both saturation points before they can die, therefore the difference in the two feedback functions affects the species both at the upper and lower boundaries. As a consequence, we do not see the same consistent effect of lower M^* as we did in the case of $a = 2$; see Fig. 7(b).

In the limit of infinite σ, both the nonlinear and piecewise linear function are effectively equivalent. In this limit all species abundances will be saturated at either boundary, $x_i = 1 + a$ or $x_i = (1 - a)\Theta(1 - a)$. The fraction of species saturated at each boundary is the same for either function, for a given γ. This results in the same limiting values for the order parameters M^* and diversity in both models.

VII. DEPENDENCE OF STABLE REGION ON MODEL PARAMETERS

In the previous section we compared results from analysis and simulations of the piecewise linear feedback to demonstrate that our theory correctly predicts the nature of the system in the regime of unique fixed points; see Fig. 3. The theory also correctly predicts the critical value of σ where this regime ends, as demonstrated in Fig. 4. We then compared predictions for the model with piecewise linear feedback with simulation results for the model with nonlinear feedback. We found a similar general dependence of the system's order parameters on σ, γ, and a; see Fig. 7. The onset of instability, σ_c, is also very similar on both models, as shown in Fig. 6. We conclude that the predictions of our theory for the piecewise linear feedback function are a good approximation to the behavior of the model with nonlinear feedback. It is therefore appropriate to use the theory we have developed to investigate further how the stability of the ecosystem with saturating nonlinear feedback depends on the key model parameters.

A. Dependence of stability on the saturation parameter *a*

We have so far shown results only for $a = 2$ and $a = 0.5$. These fall on either side of the carrying capacity which was set to one. In Fig. 8 we provide a more general picture, and show how the critical value of the heterogeneity, σ_c, depends on the saturation parameter a, and on the symmetry parameter γ. In this figure we fix the mean value $\mu = 0$ of the interaction matrix elements.

As one would expect, the range of the stable region increases as the nonlinear feedback becomes more restricted (i.e., as a is lowered). This effect is particular relevant when the saturation parameter is lower than the carrying capacity (i.e., for $a < 1$). We note that in this regime the critical strength of the heterogeneity is a decreasing function of both a and γ. For $\gamma < 0$ we also note that the stability has a similar dependence on the two parameters a and γ, which is demonstrated by the symmetry in the bottom left quadrant of Fig. 8. If the saturation parameter a exceeds the carrying capacity ($a > 1$), then its influence on the size of the stable region is small.

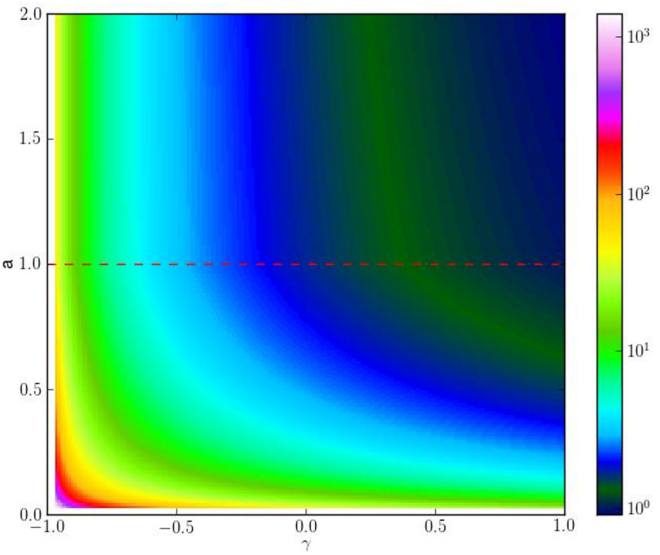

FIG. 8. Critical value of the heterogeneity parameter, σ_c, plotted as a color map in the $a - \gamma$ plane at fixed $\mu = 0$. Higher values of σ_c indicate higher stability. The dashed line indicates $a = 1$ (saturation parameter equal to carrying capacity); see text for further discussion.

B. Dependence of stability on cooperation parameter μ

We have not yet considered how stability varies with the cooperation parameter μ, i.e., the mean interacting strength between species. In the context of gut bacteria it has been argued that increasing the cooperation between species of an ecological system can reduce the system's stability [6], with higher stability found for more competitive systems.

Previous theoretical studies [24,25,37] of generalized random Lotka-Volterra systems with linear feedback have found σ_c to be independent of μ so long as $\mu \leqslant 0$. We note that the interaction term between the species carries the opposite sign in Refs. [24,25] relative to our notation, implying opposite sign conventions in particular for the parameter μ. In Refs. [24,25] a second critical value of the heterogeneity is found; if the strength of the heterogeneity exceeds this value, the system displays unbounded growth. This value is found to depend on μ, and to be equal to zero for $\mu \geqslant 1$; that is to say, when $\mu > 1$ the random generalized Lotka-Volterra system with linear feedback always exhibits unbounded growth regardless of the amount of heterogeneity.

The saturated nonlinear feedback in our model causes the abundances to be constrained to the interval $1 - a\Theta(1 - a) \leqslant x_i(t) \leqslant 1 + a$, and as a consequence the system cannot display unbounded growth. The critical value for σ, however, is now dependent on the value of μ. In Fig. 9 we show how σ_c varies with μ and γ for $a = 2$ and $a = 0.5$; these results are from numerical evaluation of the self-consistency equations obtained from the generating functional analysis.

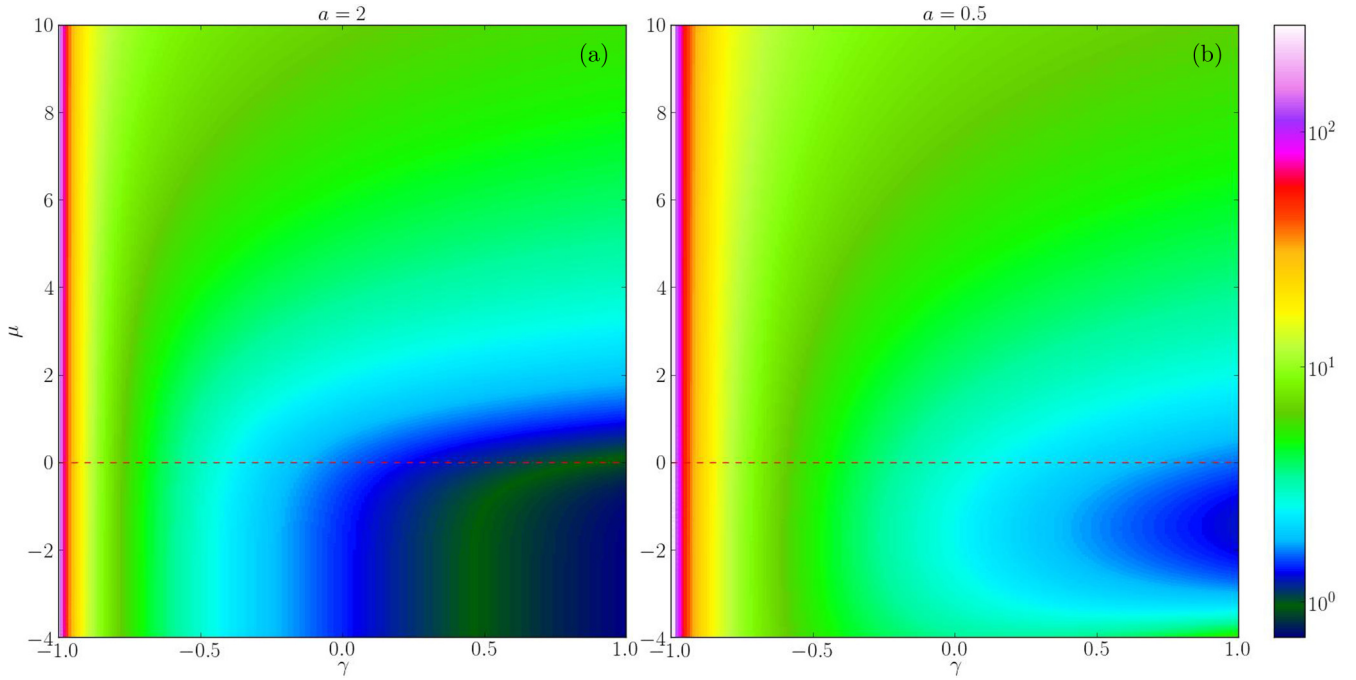

FIG. 9. Critical σ_c plotted as a color map in the $\mu - \gamma$ plane at fixed $a = 2$ (left) and $a = 0.5$ (right). Higher values of σ_c indicate higher stability. The data along the dashed line indicates values of σ_c for $\mu = 0$, these are as previously given in the black lines of Fig. 5.

For $a = 0.5$, we find a minimum value for σ_c as a function of μ, see the lower right corner of Fig. 9(b). This minimum value corresponds to a maximum proportion of unsaturated species ϕ, this is shown in Sec. S1 J and demonstrated in Fig. 10. For values of μ away from this extremal point, ϕ decreases as more species become saturated at either $1 + a$ (increasing μ) or $1 - a$ (decreasing μ), this in turn gives the system a higher stability. For $a = 2$ we also find increasing stability for higher values of μ. However, we do not find a minimum point for stability (as a function of μ). Instead σ_c monotonically decreases with decreasing μ, tending to a constant. This is because the fraction of species at the lower saturation point ($x^* = 0$ for $a = 2$) does not increase past 0.5 as μ is decreased.

The transition line shown in the μ-σ plane shown in Figs. 10(a) and 10(b) can be compared to the phase diagrams for linear feedback in Refs. [24,25,39]. For linear feedback the transition line is not dependent on μ as it is in the case of nonlinear feedback. These results are different to those found in Ref. [6], where a model with linear feedback was used, cooperation then does not promote stability. For saturating nonlinear feedback we find, instead, that stability is increased for higher values of the cooperation parameter μ.

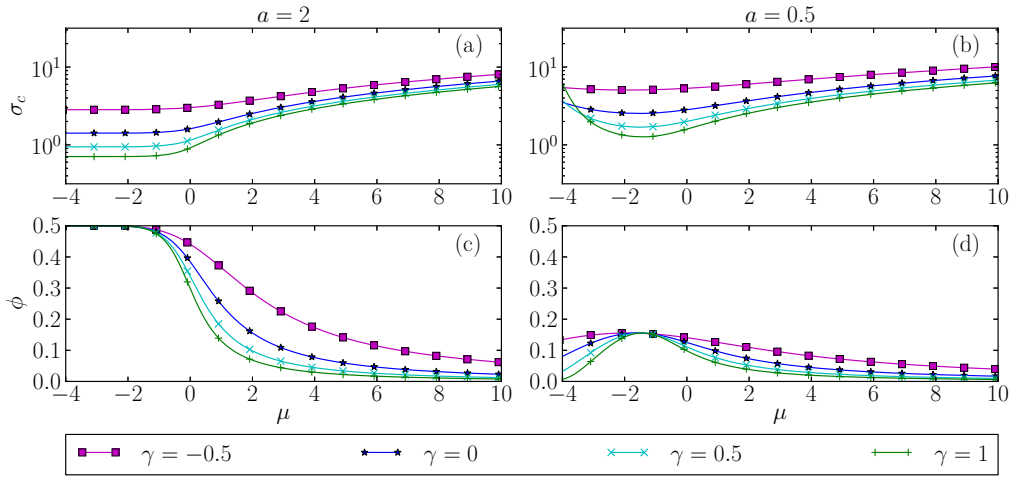

FIG. 10. Location of the onset of instability σ_c, and fraction of unsaturated species, ϕ, for varying μ at $a = 2$ (left) an $a = 0.5$ (right). Results in the figure are from the theory; the different values for γ are indicated by different symbols [$\gamma = -0.5$(■), 0(★), 0.5(×), 1(+)].

VIII. CONCLUSIONS

In summary we have analyzed generalized Lotka-Volterra communities with random interactions and nonlinear feedback. Specifically, we have studied systems in which the total feedback on the growth rate of any one species saturates via a nonlinear function. Simulations of such systems reveal three different types of behavior. When the variation in interaction coefficients is small, convergence to stable fixed points is found for a wide range of values of the remaining model parameters. These fixed points are found to be unique, in the sense that the asymptotic composition of resulting community does not depend on the starting point of the dynamics for any realization of the random interaction matrix. This globally stable behavior is found provided the heterogeneity of interactions σ does not exceed a critical value. This critical value in turn depends on the combination of the parameter a indicating saturation value, the cooperation parameter μ, and the symmetry parameter γ. Above the critical interaction heterogeneity two types of behaviours are observed: When the heterogeneity in interaction coefficients is such that it promotes symmetric interactions, we observe that the generalized Lotka-Volterra dynamics can have multiple stable fixed points, and which one is reached asymptotically depends on the choice of initial conditions. While we often find fixed points in simulations in this phase, the system could—in principle—also exhibit heteroclinic cycles for larger numbers of species N. For negatively correlated heterogeneity instead we typically observe persistently volatile dynamics.

The critical value for σ is much higher for a lower value for γ, with $\sigma_c \to \infty$ for $\gamma = -1$, when all interactions are exploitative. Low values of the saturation parameter (i.e., strongly nonlinear feedback) increases the critical σ, i.e., the range of global stability is larger. This effect is seen in particular when the saturation value a is smaller than the carrying capacity. Previous studies have found that stability decreases with an increasing cooperation parameter μ [6,24,25] in models with linear feedback. In this linear case the interaction with other species is not bounded, and a high degree of cooperation can lead to unlimited growth. With nonlinear feedback the growth of abundances is bounded, and cooperation no longer leads to unlimited growth. With nonlinear feedback we have found that increasing the cooperation parameter μ can increase stability, even when the feedback is linear over a wide range (i.e., when a is large); the key factor for stability is saturation at very large or very small arguments.

We conclude by briefly speculating about potential biological implications of our findings. The human gut has evolved with the microbiome and has adaptated to promote to stability as this is important for good health. Our findings suggest that one effective way to increase the system's global stability is to decrease γ, i.e., to exhibit more exploitative predator-prey like interactions. It may be difficult for the human gut to have an influence over the specific interactions types present between the species, as these will be a function of the microbes themselves. The human gut has however, been found to promote ecosystem stability by host feeding, immune suppression and spatial structure [6,7]. Spatial structure has the effect of reducing the interaction strength between populations of different species, which has the effect of reducing σ, which our model has shown to increase global stability. Host feeding and immune suppression may work by enforcing a bound on species population size from above and below, which may result in a similar effect produced by nonlinear feedback explored in this paper. We have shown that enforcing a tight population bound (low a) promotes ecosystem global stability but also results in a higher system diversity (Fig. 3) which is also beneficial for health. While employing nonlinear feedback, the cooperation within the system (parametrized by μ) can be increased without the adverse effect of destabilizing the system [6]. This allows a more cooperative and efficient microbiome without compromising stability. Nonlinear feedback has been observed in other ecosystems [50,51,55] and one would expect evolution to utilize this beneficial effect in the gut.

ACKNOWLEDGMENTS

We thank G. Biroli and F. Roy for discussions. L.S. acknowledges support through a PhD studentship by the Engineering and Physical Sciences Research Council (EPSRC UK), Grant No. EP/N509565/1. Partial financial support has been received from the Agencia Estatal de Investigacion (AEI, Spain) and Fondo Europeo de Desarrollo Regional (FEDER, EU) under Project PACSS (Project No. RTI2018-093732-B-C22), and the Maria de Maeztu Program for Units of Excellence in R&D (Grant No. MDM-2017-0711).

[1] C. S. Elton, *The Ecology of Invasions by Animals and Plants* (University of Chicago Press, Chicago, 2000).
[2] R. Macarthur, Ecology **36**, 533 (1955).
[3] M. R. Gardner and W. R. Ashby, Nature **228**, 784 (1970).
[4] R. M. May, Nature **238**, 413 (1972).
[5] R. M. May, *Stability and Complexity in Model Ecosystems* (Princeton University Press, Princeton, NJ, 1973).
[6] K. Z. Coyte, J. Schluter, and K. R. Foster, Science **350**, 663 (2015).
[7] K. R. Foster, J. Schluter, K. Z. Coyte, and S. Rakoff-Nahoum, Nature **548**, 43 (2017).
[8] S. Allesina and M. Pascual, Theor. Ecol. **1**, 55 (2008).
[9] S. Allesina and S. Tang, Nature **483**, 205 (2012).
[10] S. Allesina and S. Tang, Popul. Ecol. **57**, 63 (2015).
[11] S. Tang, S. Pawar, and S. Allesina, Ecol. Lett. **17**, 1094 (2014).
[12] J. Grilli, T. Rogers, and S. Allesina, Nature Commun. **7**, 12031 (2016).
[13] T. Gibbs, J. Grilli, T. Rogers, and S. Allesina, Phys. Rev. E **98**, 022410 (2018).
[14] M. L. Mehta, *Random Matrices*, Pure and Applied Mathematics Vol. 142 (Elsevier Science Limited, Amsterdam, 2004).
[15] W. Post and S. Pimm, Math. Biosci. **64**, 169 (1983).
[16] A. G. Rossberg, *Food Webs and Biodiversity* (Wiley-Blackwell, Chichester, West Sussex, UK, 2013).
[17] M. Opper and S. Diederich, Phys. Rev. Lett. **69**, 1616 (1992).

[18] M. Mezard, G. Parisi, and M. A. Virasoro, *Spin Glass Theory and Beyond* (World Scientific, Singapore, 1993).
[19] J. Berg and A. Engel, Phys. Rev. Lett. **81**, 4999 (1998).
[20] J. Berg and M. Weigt, Europhys. Lett. **48**, 129 (1999).
[21] S. Diederich and M. Opper, Phys. Rev. A **39**, 4333 (1989).
[22] P. Biscari and G. Parisi, J. Phys. A: Math. Gen. **28**, 4697 (1995).
[23] V. M. de Oliveira and J. Fontanari, Phys. Rev. Lett. **85**, 4984 (2000).
[24] G. Bunin, arXiv:1607.04734 (2016).
[25] G. Bunin, Phys. Rev. E **95**, 042414 (2017).
[26] G. Biroli, G. Bunin, and C. Cammarota, New J. Phys. **20**, 083051 (2018).
[27] C. De Dominicis, Phys. Rev. B **18**, 4913 (1978).
[28] P. C. Martin, E. D. Siggia, and H. A. Rose, Phys. Rev. A **8**, 423 (1973).
[29] H. J. Sommers, A. Crisanti, H. Sompolinsky, and Y. Stein, Phys. Rev. Lett. **60**, 1895 (1988).
[30] A. C. C. Coolen, Statistical mechanics of recurrent neural networks II—Dynamics, in *Neuro-Informatics and Neural Modelling*, edited by F. Moss and S. Gielen, Vol. 4 of Handbook of Biological Physics (North-Holland, Amsterdam, 2001), Chap. 15, pp. 619–684.
[31] A. C. C. Coolen, *The Mathematical Theory of Minority Games: Statistical Mechanics of Interacting Agents* (Oxford University Press, Oxford, 2005).
[32] J. A. Hertz, Y. Roudi, and P. Sollich, J. Phys. A: Math. Theor. **50**, 033001 (2016).
[33] T. Galla, J. Phys. A: Math. Gen. **39**, 3853 (2006).
[34] T. Galla, J. Stat. Mech.: Theory Exp. (2005) P11005.
[35] Y. Yoshino, T. Galla, and K. Tokita, J. Stat. Mech.: Theory Exp. (2007) P09003.
[36] Y. Yoshino, T. Galla, and K. Tokita, Phys. Rev. E **78**, 031924 (2008).
[37] T. Galla, Europhys. Lett. **78**, 20005 (2007).
[38] H. Eissfeller and M. Opper, Phys. Rev. Lett. **68**, 2094 (1992).
[39] F. Roy, G. Biroli, G. Bunin, and C. Cammarota, J. Phys. A: Math. Gen. **52**, 484001 (2019).
[40] V. Domínguez-García, V. Dakos, and S. Kéfi, Proc. Natl. Acad. Sci. U.S.A. **116**, 25714 (2019).
[41] V. Grimm and C. Wissel, Oecologia **109**, 323 (1996).
[42] J. D. O'Sullivan, R. J. Knell, and A. G. Rossberg, Ecol. Lett. **22**, 1428 (2019).
[43] T. Galla, Europhys. Lett. **123**, 48004 (2018).
[44] Y. Sato and J. P. Crutchfield, Phys. Rev. E **67**, 015206(R) (2003).
[45] T. Galla and J. D. Farmer, Proc. Natl. Acad. Sci. U.S.A. **110**, 1232 (2013).
[46] A. V. Hill, J. Physiol. **40**, i (1910).
[47] C. S. Holling, Memoirs Entomol. Soc. Canada **97**, 5 (1965).
[48] G. Bunin, bioRxiv: 484576 (2019).
[49] D. H. Boucher, S. James, and K. H. Keeler, Annu. Rev. Ecol. Syst. **13**, 315 (1982).
[50] C. S. Holling, Can. Entomol. **91**, 293 (1959).
[51] C. S. Holling, Can. Entomol. **91**, 385 (1959).
[52] See Supplemental Material at http://link.aps.org/supplemental/10.1103/PhysRevE.101.032101 for additional details of analytical calculations and computer simulations
[53] M. Barbier and J.-F. Arnoldi, bioRxiv: 147728 (2017).
[54] E. H. Simpson, Nature **163**, 688 (1949).
[55] L. A. Real, Ecology **60**, 481 (1979).